Appl. Phys. A (2016) 122:20
DOI 10.1007/s00339-015-9551-z

Applied Physics A
Materials Science & Processing

Structural, linear and nonlinear optical properties of co-doped ZnO thin films

E. R. Shaaban[1] · M. El-Hagary[2] · El Sayed Moustafa[1] · H. Shokry Hassan[3] · Yasser A. M. Ismail[1] · M. Emam-Ismail[4] · A. S. Ali[1]

Received: 13 October 2015 / Accepted: 15 December 2015 / Published online: 24 December 2015

Abstract Different compositions of Co-doped zinc oxide [$(Zn_{(1-x)}Co_xO)$ ($x = 0$, 0.02, 0.04, 0.06, 0.08 and 0.10)] thin films were evaporated onto highly clean glass substrates by thermal evaporation technique using a modified source. The structural properties investigated by X-ray diffraction revealed hexagonal wurtzite ZnO-type structure. The crystallite size of the films was found to decrease with increasing Co content. The optical characterization of the films has been carried out using spectral transmittance and reflectance obtained in the wavelength range from 300 to 2500 nm. The refractive index has been found to increase with increasing Co content. It was further found that optical energy gap decreases from 3.28 to 3.03 eV with increasing Co content from $x = 0$ to $x = 0.10$, respectively. The dispersion of refractive index has been analyzed in terms of Wemple–DiDomenico (WDD) single-oscillator model. The oscillator parameters, the single-oscillator energy (E_o), the dispersion energy (E_d), and the static refractive index (n_0), were determined. The nonlinear refractive index of the $Zn_{(1-x)}Co_xO$ thin films was calculated and revealed well correlation with the linear refractive index and WDD parameters which in turn depend on the density and molar volume of the system.

✉ E. R. Shaaban
esam_ramadan2008@yahoo.com

[1] Department of Physics, Faculty of Science, Al-Azhar University, Asyût 71452, Egypt

[2] Department of Physics, Faculty of Science, Helwan University, Helwan, Cairo 11792, Egypt

[3] Technology and New Materials Research Institute, City of Scientific Research and Technology Applications, New Borg El-Arab City, Alexandria 21934, Egypt

[4] Physics Department, Faculty of Science, Ain Shams University, Cairo 11566, Egypt

1 Introduction

Zinc oxide (ZnO) has a wide-band-gap (3.37 eV) wurtzite phase semiconductor. In order to obtain different properties and applications for ZnO, researchers carried out doping in ZnO. Doping of ZnO by impurity atoms achieved their widespread technological applications in microelectronics and optoelectronics [1], and nanocrystals doped with magnetic impurities are of interest for their potential use in spin-based electronic devices [2]. On this account, diluted magnetic semiconductors (DMSs) have caused extensive scientific concerns because of their potential applications in spintronics and optoelectronics [3–7]. TM-doped ZnO has been theoretically proved to be one of the most promising materials for room temperature ferromagnetism [8–14]. In recent past, cobalt (Co) and other transition metal (TM)-doped ZnO nanomaterials have a focus for many researchers [15, 16]. However, among numerous reports on $Zn_{1-x}Co_xO$ thin films, very few have been published on morphology design of thin films, which is of special interest as building blocks for the applications of DMSs, such as spintronic, electro-optical devices, and microwave absorbing materials [17]. The visible photo-response of Co-doped ZnO has been observed by many researchers using single crystals [18] or polycrystalline of Co^{2+}:ZnO prepared by pellet sintering [19]. Zhang and coworkers [20] reported a template-free solvothermal method for the formation of TM-doped ZnO spheres and hollow spheres. They found that the Co-doped ZnO hollow exhibited ferromagnetism at room temperature, whereas nickel-doped ZnO hollow spheres exhibited only weak ferromagnetism

at 300 K. Bhattacharyya and Gedanken [21] found that the size of ZnO nanocrystals varied with the variation in cobalt concentration. In the present study, Co-doped ZnO ($Zn_{1-x}Co_xO$, $x = 0$, 0.02, 0.04, 0.06, 0.08, and 0.10) are fabricated using chemical co-precipitation method. Thin films of $Zn_{1-x}Co_xO$ with various Co concentrations are deposited by thermal evaporation using a modified source. The effect of doping concentration on structural, linear, and non-linear optical properties of $Zn_{1-x}Co_xO$ thin films is investigated.

2 Experimental

The bulk samples of $Zn_{1-x}Co_xO$ ($x = 0$, 0.02, 0.04, 0.06, 0.08, and 0.1) are prepared by using co-precipitation technique of $Zn(NO_3)_2{\cdot}6H_2O$ with appropriate amount of $Co(NO_3)_2{\cdot}6H_2O$ to make desired doping percentage dissolved in 50 ml of distilled water. Zinc and cobalt nitrates are dissolved in deionized water to get a solution and then kept stirring for 1 h. Then, NH_4OH solution is added drop wise until the pH of the solution has reached 9. This mixture is stirred for 3 h at room temperature and, consequently, filtered. The precipitate is dried at 80 °C for 5 h. The thermal behavior of the precursor is analyzed by thermogravimetric analysis (TGA) (Shimadzu 50 with an accuracy of ±0.1 K). Finally, the dried samples are grounded and kept for calcination at 480 °C for 2 h, in order to obtain polycrystalline powder. Thin films of $Zn_{1-x}Co_xO$ with various Co concentrations ($x = 0$, 0.02, 0.04, 0.06, 0.08, and 0.1) are deposited by thermal evaporation using a modified source. This modified source is a resistive-heated quartz crucible containing $Zn_{1-x}Co_xO$ powders and wrapped in a tantalum sheet. This arrangement was found to facilitate the loading of $Zn_{1-x}Co_xO$ powder and increase the lifetime of the heater. A small wad of quartz fiber wool is placed in the neck of quartz crucible to prevent spattering of powdered samples during outgassing and evaporation. This modified source has been proven to produce the films with high quality. The glass substrates are fixed onto substrate holder inside vacuum chamber at a distance of about 20 cm above the evaporation source of the conventional coating unit (Denton 306A) with a vacuum of about 10^{-6} Pa. The evaporation rate as well as film thickness is controlled using a quartz crystal FTM6 monitor. The deposition rate is maintained constant at 10 Å/s throughout the sample preparation. Such a low deposition rate can produce a film with a composition which is very close to that of the bulk starting material.

The structure of the prepared samples in the form of powders and thin films is examined by X-ray diffraction (XRD) analysis [Shimadzu X-ray diffractometry 6000 (Japan) with CuKα radiation having $\lambda = 0.15418$ nm]. The intensity data are collected by step scan modes of a 2θ range between 10 and 70 with step size of 0.02° and step time of 0.6 s. The pure silicon (≈Si 99.9999 %) is used as an internal standard. The composition of the synthesized polycrystalline particles is quantified by energy-dispersive analysis of X-ray (EDAX) using energy-dispersive X-ray (EDX) spectrometer attached to scanning electron microscopy (SEM; JEOL JSM-6360LA, Japan), operating with an accelerating voltage of 30 kV. EDX technique is based on the evaluation of the X-ray energies emitted by a sample impacted by the fast-moving primary electrons in the SEM. It allows one to identify and quantify the chemical compounds within a depth of about 1 μm [22], which depends on the acceleration voltage of the primary electron beam and on the chemical composition. Phase identification and quantification depend on the accurate measurement of the value and intensity of the different peaks of the X-ray energy spectra. Quantitative determination is carried out by comparing the integrated intensities of selected peaks (i.e., those who have the best number of counts, for a given time, like the Kα ones in our case) with standard X-ray data for reference materials [23]. These spectra can be measured at different locations of the sample surface. More details about elemental compositions using EDX were in the two references [22, 23].

Transmission electron microscope (TEM) micrographs are taken using a JEOL JEM 1230, Japan. Samples are dispersed in methanol by sonication and placed on the copper grid for TEM investigation. The optical transmittance (T) and reflectance (R) of the deposited films are measured using a UV–Vis-NIR JASCO V-670 double-beam spectrophotometer. The transmittance spectra in the wavelength range of 400–2500 nm are collected at normal incidence without a substrate in the reference beam, whereas the reflectance spectra are measured using a reflection attachment close to normal incidence (∼5°). In our measurements of the R and T, the effect of slit correction is eliminated by the adjust of the spectrophotometer slit width to be 6 mm, which is much less than the width of the interference peaks observed in the transparent region of the investigated samples.

3 Results and discussion

3.1 Structural properties

The TGA is performed to study the change in the phases during crystallization. The simultaneous TGA graph and its differentiation are shown in Fig. 3. The differentiation of TGA curve is very important for identifying the peaks with high precision. The first peak was observed at 87.2 °C, which represents the mass loss due to evaporation of

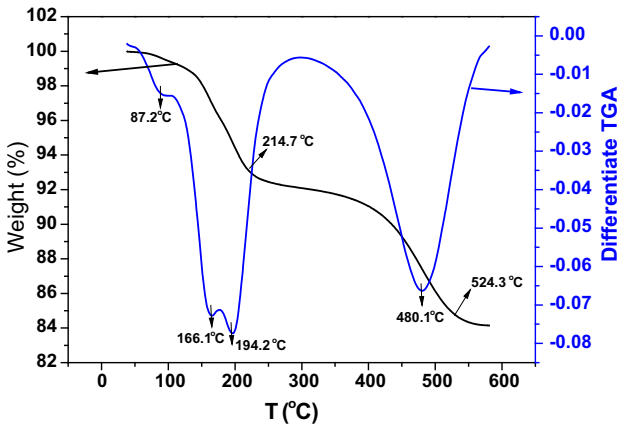

Fig. 1 Simultaneous TGA and its differentiation curves for $Zn_{0.94}Co_{0.06}O$ precursor

ethanol. This behavior can be observed from both mass loss graph and its differentiation. The second downward peak in the heat flow graph and the further decrease in the mass is observed at 166.1 and 194.2 °C in the weight curve, which represent the decompositions of $Zn(OH)_2$ and $Co(OH)_2$, respectively. Both the materials liberate water molecules under successive temperature. The 10 % mass loss is further observed at approximately 480.1 °C due to crystallization of the ZnO (Fig. 1).

The purity and crystallinity of the as-synthesized ZnO polycrystalline are examined by using XRD of the powder, as shown in the upper curve in Fig. 2. The lower curve in Fig. 2 represents a simulate scan from the pattern according to Ref. Code 01-1136 cards using X'Pert HighSore (version 1.0e) program.

Figure 3 shows XRD of the as-deposited $Zn_{1-x}Co_xO$ thin films with variation of Co concentration ($x = 0$, 0.02, 0.04, 0.06, 0.08, and 0.1). All of the diffraction peaks, which correspond to the planes (1 0 0), (0 0 2), (1 0 1), (1 0 2), and (1 0 0), are perfectly indexed to the hexagonal wurtzite ZnO structure (JCPDS 01-1136), revealing that the doping of Co does not change the crystal structure of the ZnO.

The absence of the individual metal (Co) or Co-related impurity phase diffraction peaks in the XRD patterns confirms the formation of the $Zn_{1-x}Co_xO$ solid solution. Furthermore, all the films exhibit preferential orientation along (002) plane. Figure 3, also, shows that the intensity of the ZnO peaks decreases with increasing Co concentration. It is also observed in Fig. 3 a very small shift of the position of the diffraction peak (002) toward lower values of the diffraction angle (2θ). This small shift in the peak position is due to higher ionic radii of Co^{2+} ions (0.078 nm) relative to the ionic radii of Zn^{2+} ions (0.074 nm). The lattice strain (ε) parameter is calculated using the following relation [24, 25]:

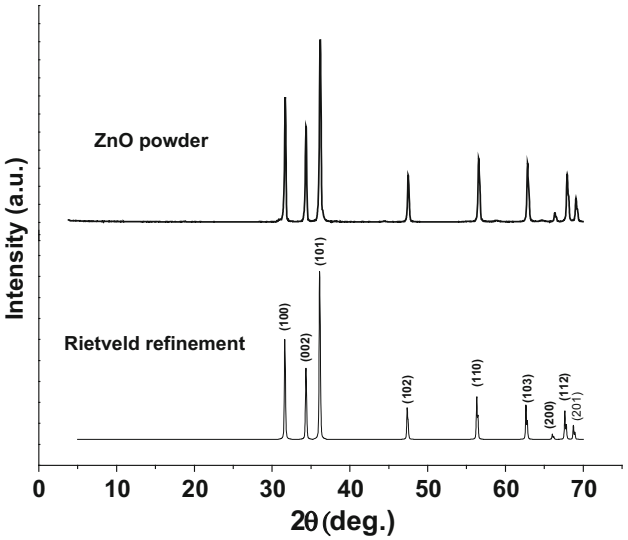

Fig. 2 (*upper curve*) XRD pattern of the ZnO powder and (*lower curve*) a simulate scan from the pattern according to Ref. Code 01-1136 cards using X'Pert HighSore (version 1.0e) program

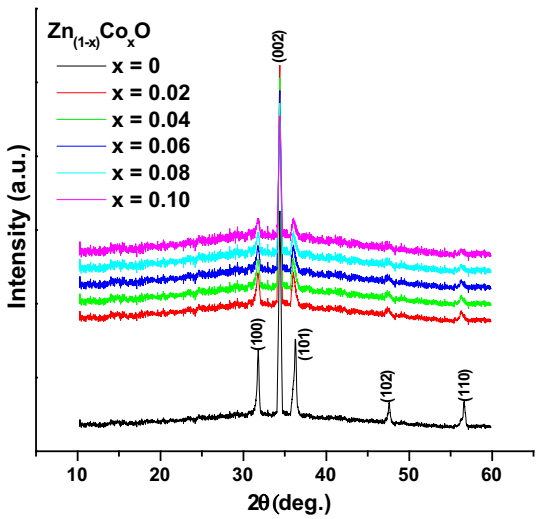

Fig. 3 XRD patterns of $Zn_{1-x}Co_xO$ thin films with different Co compositions ($x = 0$, 0.02, 0.04, 0.06, 0.08, and 0.1)

$$\varepsilon = \frac{\beta}{4\tan(\theta)} \tag{1}$$

where θ is the Bragg's diffraction angle of the peak and β is breadth of the peak, which describes the structural broadening and is calculated through the formula:

$$\beta = \sqrt{\beta_{\text{obs}}^2 - \beta_{\text{std}}^2} \tag{2}$$

where β_{obs} is the integral peak profile width of the sample and β_{std} is the peak profile width of standard (silicon). In addition, from XRD patterns, the crystallite size of the

films is calculated by using the well-known Debye–Scherrer's formula [24, 25]:

$$D_v = \frac{k\lambda}{\beta\cos(\theta)} \tag{3}$$

where λ is the wavelength (1.54 Å). Assuming that the particle size and strain contributions to line broadening are independent to each other and both have a Cauchy-like profile, the observed line breadth is simply the sum of Eqs. (1) and (2). Then, we get the formula:

$$\beta(2\theta)\cos\theta_0 = \frac{k'\lambda}{D_v} + 4e(\sin\theta_0) \tag{4}$$

Equation (4) is customarily referred to as the "Williamson–Hall method" [26–28]. Figure 4 illustrates $\sin(\theta_0)$ along the x-axis and $\beta(2\theta)$ $\cos(\theta_0)$ along the y-axis for different compositions of the $Zn_{1-x}Co_xO$ thin films. The values of the crystallite size (D_v) and the lattice strain (ε) can be estimated from the slope and the ordinate intersection, respectively. Table 1 shows the microstructure parameters (D_v and ε) of the pure ZnO and $Zn_{1-x}Co_xO$ films deposited on glass substrates. It is clear that the crystallite size decreases and the lattice strain increases with increasing Co content in the $Zn_{1-x}Co_xO$ films. Such the increase in the lattice strain and the decrease in the crystallite size reflect the increase in concentration of lattice imperfections due to addition of Co to the ZnO.

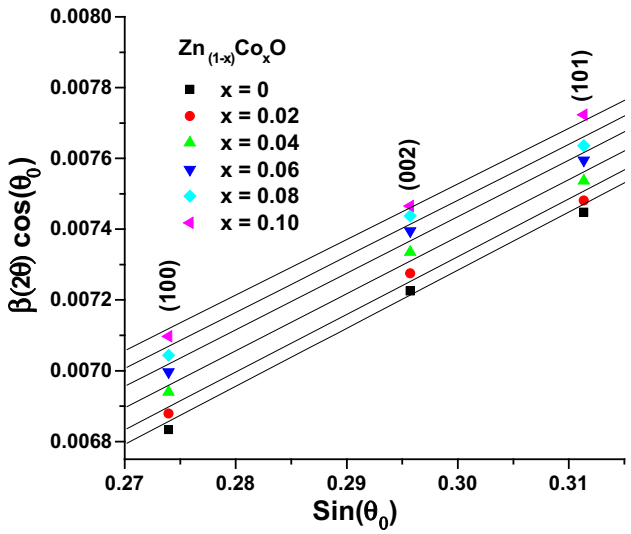

Fig. 4 Crystallite size/strain separation calculating using the breadth according to "Williamson–Hall" method

Energy-dispersive X-ray analysis (EDAX) measurement is taken in order to confirm the presence of Co^{2+} in the synthesized $Zn_{0.94}Co_{0.06}O$ polycrystalline particles and to determine their compositions. EDAX spectra displayed in Fig. 5 demonstrate the presence of various elements in the prepared doped samples. The EDAX analysis provides precise composition of the elements. The EDAX spectra in Fig. 5 show peaks corresponding to elements of Zn, O, and Co for $Zn_{0.94}Co_{0.06}O$ sample. TEM studies have also been checked for the thin film sample $Zn_{0.94}Co_{0.06}O$. Figure 6a shows the TEM image of $Zn_{0.94}Co_{0.06}O$ thin film. TEM images reveal that all nanostructure has the same hexagonal morphology, approximately. The histogram is given in Fig. 6b. The mean particle size is found to be 58 nm, which agrees with that obtained from XRD calculation using Williamson–Hall method.

3.2 Optical properties

3.2.1 Determination of optical constants

The absolute values of the measured transmittance $T(\lambda)$ and reflectance $R(\lambda)$ are given according to the following equations [29, 30]:

$$T = \left(\frac{I_{ft}}{I_g}\right)(1 - R_g) \tag{5}$$

where I_{ft} and I_g are the intensities of the light passing through the film/glass substrate and the reference glass substrate, respectively.

$$R = \left(\frac{I_{ft}}{I_{A1}}\right)R_{A1}\left[1 + (1 - R_g)^2\right] - T^2R_g \tag{6}$$

Table 1 Values of microstructure parameters, energy gap, dispersion parameters, nonlinear parameters, density, molar volume, and density of polarizable constituents as a function of Co content of the $Zn_{1-x}Co_xO$

$Zn_{1-x}Co_xO$	D_v (nm)	e × 10^{-3}	E_g^{opt} (eV)	E_d (eV)	E_o (eV)	n(o)	χ_1	χ_3 × 10^{-13}	n_{o2} × 10^{-13}	ρ (g/cm^3)	V_m (g mol^{-1})	N × 10^{22}
0	65.36	3.93	3.28	9.566	6.534	1.57	0.117	0.313	1.254	5.93	13.383	4.431
0.02	63.41	3.96	3.24	10.446	6.382	1.624	0.13	0.489	1.893	5.955	13.313	4.473
0.04	60.73	3.99	3.19	11.281	6.332	1.668	0.142	0.687	2.587	5.98	13.243	4.516
0.06	58.3	4.04	3.14	12.069	6.374	1.701	0.151	0.877	3.238	6.005	13.173	4.559
0.08	56.44	4.08	3.10	13.475	6.184	1.783	0.173	1.536	5.414	6.03	13.104	4.602
0.10	54.72	4.11	3.03	15.115	6.014	1.874	0.2	2.72	9.117	6.055	13.035	4.645

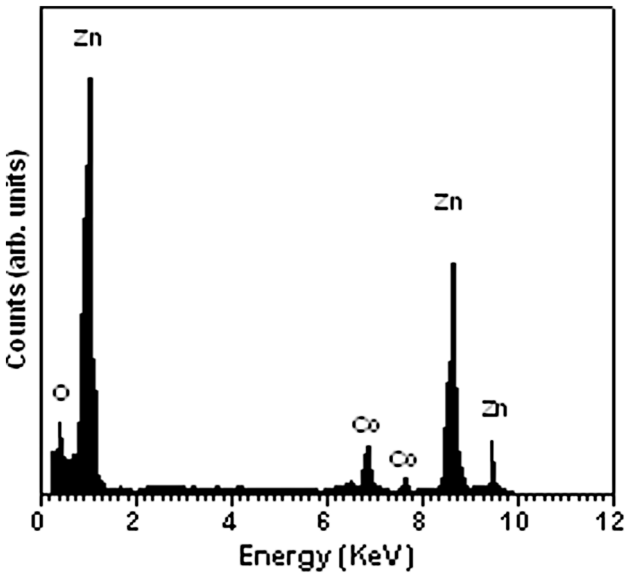

Fig. 5 Typical EDXS spectra of the $Zn_{0.94}Co_{0.06}O$ thin film

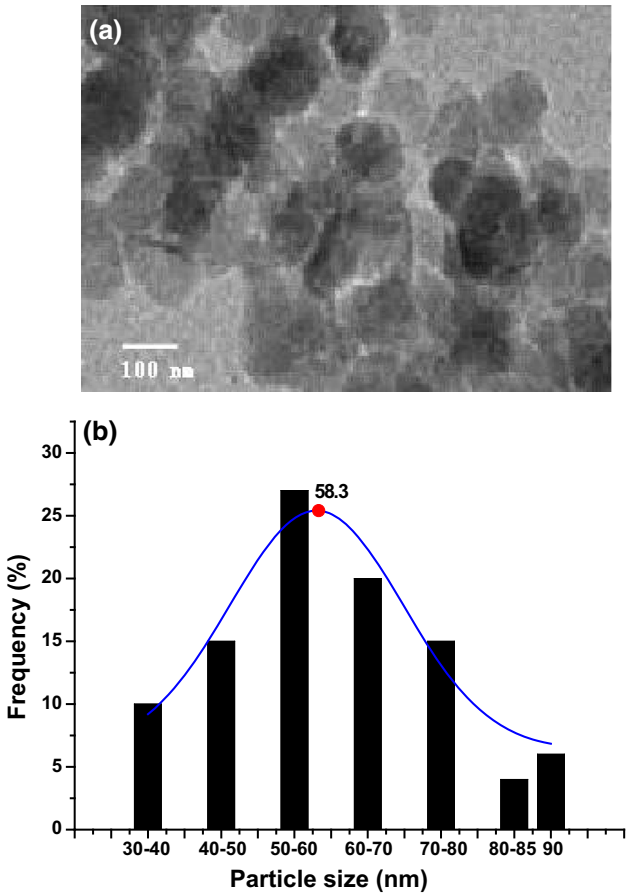

Fig. 6 **a** Representative TEM micrograph of the $Zn_{0.94}Co_{0.06}O$ thin film and **b** histogram for $Zn_{0.94}Co_{0.06}O$ thin film giving average size of 58.3 nm

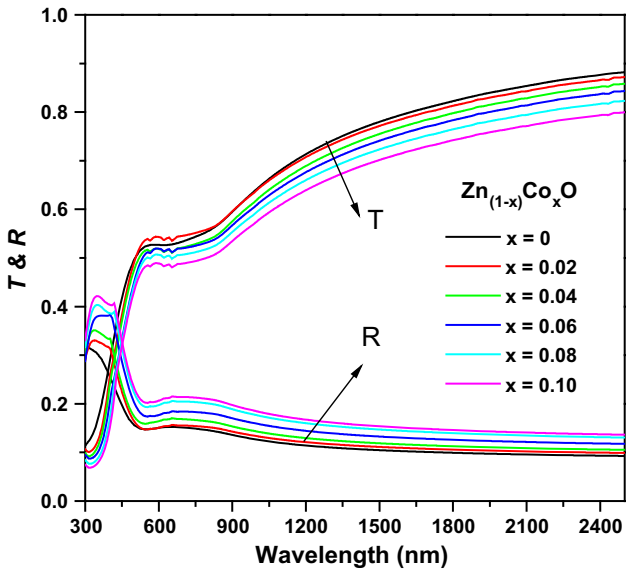

Fig. 7 Variation of the absolute values of $T(\lambda)$ and $R(\lambda)$ against wavelength (λ) for the $Zn_{1-x}Co_xO$ thin films at different Co compositions ($x = 0$, 0.02, 0.04, 0.06, 0.08, and 0.1)

where I_{fr} and I_{Al} are the intensities of the light reflected from sample and from reference mirror, respectively, while R_g is the reflectance of glass. The variation of the absolute values of $T(\lambda)$ and $R(\lambda)$ versus wavelength (λ) for the as-deposited films of the $Zn_{1-x}Co_xO$ thin films at different Co contents is shown in Fig. 7. All the samples show a sharp fall in transmittance at the fundamental absorption band edge. This sharp edge corresponds to electron excitation from the valance band to conduction band and interrelated to the nature and value of the optical band gap. A remarkable shift of the absorption edge toward higher wavelengths (redshift) with increasing Co content is observed. According to the fundamental Kramers–Kronig relations, the redshift in the spectral distribution must necessarily give an increased refractive index value (see later).

For determination of the optical constants; refractive index (n) and extinction coefficient (k), a method comprised a search technique based on minimizing $(\Delta T)^2$ and $(\Delta R)^2$ simultaneously has been used, where

$$(\Delta R)^2 = \left|R_{calc}(n,k,d,\lambda) - R_{exp}\right|^2 \quad (7)$$

$$(\Delta T)^2 = \left|T_{calc}(n,k,d,\lambda) - T_{exp}\right|^2 \quad (8)$$

T_{exp} and R_{exp} are the experimentally determined values of the T and R, respectively, while T_{calc} and R_{calc} are the calculated values of the T and R, using Murmann's exact equation [31]. The adapted computation steps are as follows:

- The T_{exp}, R_{exp}, d, and n are entered.
- The d is an important parameter in the accurate determination of the optical constant. Therefore,

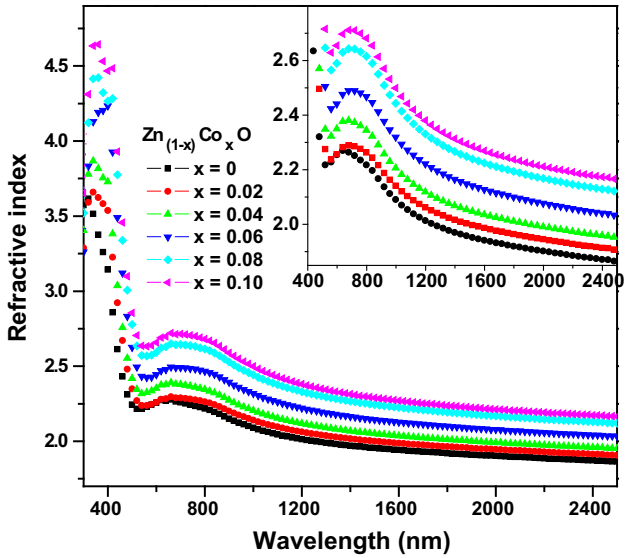

Fig. 8 Refractive index (n) versus wavelength (λ) of the $Zn_{1-x}Co_xO$ thin films at different Co compositions ($x = 0$, 0.02, 0.04, 0.06, 0.08, and 0.1)

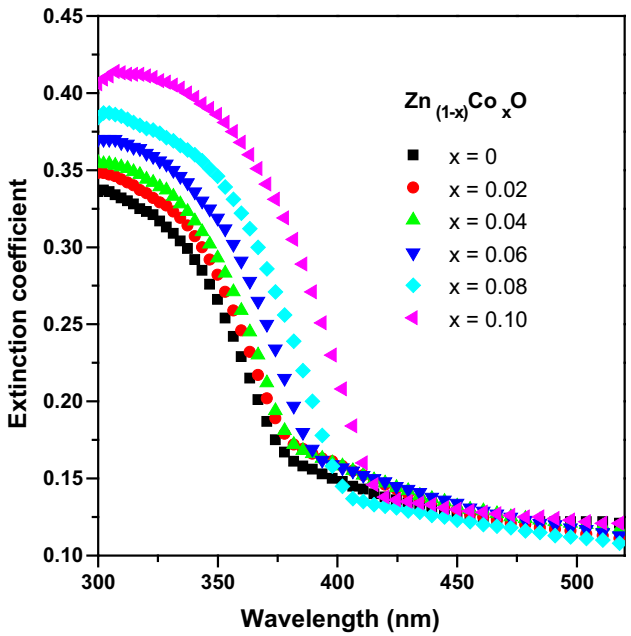

Fig. 9 Extinction coefficient (k) versus wavelength (λ) of the $Zn_{1-x}Co_xO$ thin films at different Co compositions ($x = 0$, 0.02, 0.04, 0.06, 0.08, and 0.1)

different methods have been used for determination of the thickness of the deposited films. Such thickness has been firstly estimated in situ by using a quartz crystal thickness monitor pre-calibrated interferometrically by using multiple beams Fizeau fringes at reflection [32].

- There are ranges of the n and k within which the optimal solution is expected. The desired accuracy in n and k is set up as increments in the n and k, respectively.
- Using the Murmann's equation [31], both T_{calc} and R_{calc} are calculated throughout the whole ranges.
- In each step, the variances of $(\Delta T)^2$ and $(\Delta R)^2$ are calculated and compared to seek their simultaneous minimization. The corresponding values of n and k represent the solution. During the iteration, in some small regions of the spectrum, the solutions may be missed. The missed part can be interpolated by using the program origin version 7 (OriginLab Corp.).

The optical constants, n and k, of $Zn_{1-x}Co_xO$ thin films with different compositions ($x = 0$, 0.02, 0.04, 0.06, 0.08, and 0.10) are shown in Figs. 8 and 9, respectively.

It can be seen that both of optical constants, n and k, increase with increasing Co concentration in the strong absorption region. The observed increase in n with increasing Co content may be attributed to the increase in polarizability. The atomic radii of Zn and Co are 1.53 and 1.67 Å, respectively [21]. The larger atomic radius of the atom, the larger will be its polarizability. Therefore, such dependence of the n on Co content of the investigated films can be explained on the basis of Lorentz–Lorenz equation in which a direct proportion between polarizability and n is established [33]. Thus, substituting more polarized Co atoms by less polarized Zn may lead to an increase in n.

3.2.2 *Determination of dispersion parameters*

The spectral dependence data of the refractive index dispersion of the $Zn_{1-x}Co_xO$ thin films (as deposited) with different Co contents ($x = 0$, 0.02, 0.04, 0.06, 0.08, and 0.10) can be evaluated according to the single-effective-oscillator model proposed by Wemple–DiDomenico (WDD) [34]. The model suggests that the n of the films can be correlated with oscillator energy (E_o) and dispersion energy (E_d) by the following formula:

$$n^2 = 1 + \frac{E_o E_d}{E_o^2 - (h\nu)^2} \tag{9}$$

where $h\nu$ is the photon energy, while E_o and E_d are single-oscillator constants.

Figure 10 shows optical dispersion behavior $(n^2 - 1)^{-1}$ versus $(h\nu)^2$, for the investigated thin films. The oscillator parameters E_o and E_d are determined by fitting a straight line to the points. The slope of the linear relation represents $(E_o E_d)^{-1}$, while the intercept with the vertical axis equals to (E_o/E_d).

The obtained values of the dispersion parameter (E_o) and (E_d) of the (as-deposited) $Zn_{1-x}Co_xO$ films are listed in Table 1. Furthermore, the E_o (or the effective oscillator energy) can be directly correlated with the optical energy gap (E_g^{opt}) by an empirical formula: $E_o = 2 \times E_g^{opt}$, as stated by Tanaka [35]. The dispersion energy (or oscillator

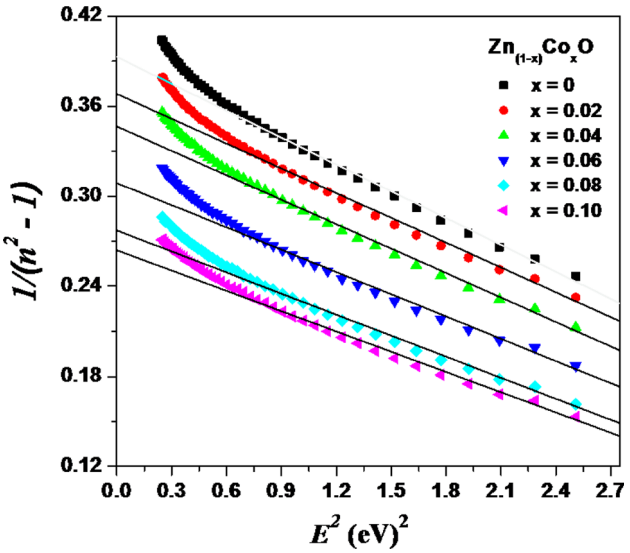

Fig. 10 Optical dispersion behavior $(n^2 - 1)^{-1}$ against $(h\nu)^2$, for the investigated $Zn_{1-x}Co_xO$ thin films

strength) follows a simple empirical relation: $E_d = \beta N_c Z_a N_e$, where β is a constant having two values of either 0.26 ± 0.03 eV for ionic materials or 0.37 ± 0.04 eV for covalent materials [36], N_c is the coordination number of the cation nearest neighbor to the anion (≅4 for $Zn_{1-x}Co_xO$), Z_a is the formal chemical valence of the anion, and N_e is the total number of valence electrons (core electrons are excluded) per anion which is calculated from the above empirical formula (see Table 1). It is found that the N_e is identical ($N_e = 8$) with increasing Co content. It is obviously found that the E_o decreases, while the E_d increases with increasing Co content. The decrease in the oscillator energy with composition may be attributed to the observed shift of optical transmission spectra in the short wavelength region, where the absorption edge is shifted toward lower energies.

Further analysis of the $(n^2 - 1)^{-1}$ against $(h\nu)^2$ allows to determine the static refractive index using the following relation:

$$n_o = (1 + E_d/E_0)^{1/2} \tag{10}$$

By extrapolating the WDD dispersion relation to the value of the incident $h\nu$ approaching zero. The calculated values of the static refractive index (n_o) for all the investigated films are listed in Table 1. It is observed that the n_o increases with increasing Co content. Similar behavior of the variation of n_0 with Mn concentration in $Zn_{1-x}Mn_xS$ system has been reported [37].

3.2.3 Nonlinear refractive index

When high-intensity light propagates through the medium, it causes nonlinear effects. The nonlinear refractive index (n_2) is highly dependent on the incident intensity. When matter is exposed to intense electric field of the incident light, the polarization is no longer proportional to electric field, and the change in polarizability has to be extended by the terms which are proportional to square of electric field [38]. The n_2 is calculated in terms of Tichy and Ticha relation [39] and Fourier and Snitzer relation [40].

3.2.3.1 Tichy and Ticha relation Tichy and Ticha relation is a combination of Miller's generalized rule and n_o obtained from WDD model [39] in the form:

$$n_{o2} = \frac{12\pi\chi^{(3)}}{n_o} \tag{11}$$

where $\chi^{(3)}$ is the third-order nonlinear susceptibility, which is obtained from the relation [41]:

$$\chi^{(3)} = A(\chi^{(1)})^4 \tag{12}$$

where $\chi^{(1)}$ is the linear susceptibility, which is given as:

$$\chi^{(1)} = \frac{E_d}{4\pi E_o} \tag{13}$$

where $A = 1.7 \times 10^{-10}$ (for $\chi^{(3)}$ in esu). Then, $\chi^{(3)}$ is given as:

$$\chi^{(3)} = \frac{A}{(4\pi)^4}\left(n_o^2 - 1\right)^4 \tag{14}$$

The values of n_2, $\chi^{(1)}$, and $\chi^{(3)}$ are given in Table 1. From this table, it is found that the values of n_{o2} and $\chi^{(3)}$ increase with increasing Co content.

3.2.3.2 Fournier and Snitzer relation Fournier and Snitzer [40] had proposed a formulation to determine n_2 on the basis of n and WDD parameters (E_o, E_d) using the following relation:

$$n_2 = \frac{(n^2 + 2)^2(n^2 - 1)}{48\pi n N}\frac{E_d}{E_o^2} \tag{15}$$

where N is the density of polarized constituents (calculated by making use of density/molar volume data). The n_2 is calculated in esu (for unit conversions, see Refs. [42, 43]). The density of the system is calculated theoretically by using the following relation:

$$\rho = \frac{x\rho_{Zn} + y\rho_{Co} + z\rho_O}{100} \tag{16}$$

From the density data, we have calculated the molar volume given by the formula:

$$V_m = \frac{1}{\rho}\sum_i X_i M_i \tag{17}$$

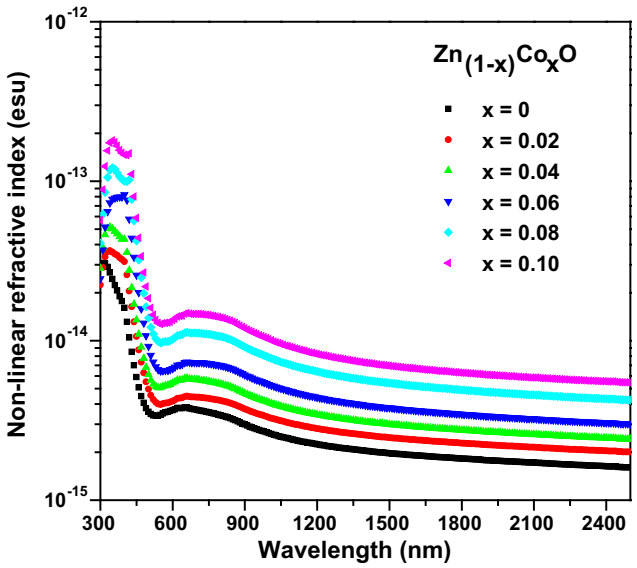

Fig. 11 Variation of nonlinear refractive index (n_2) with wavelength (λ) for the $Zn_{1-x}Co_xO$ thin films

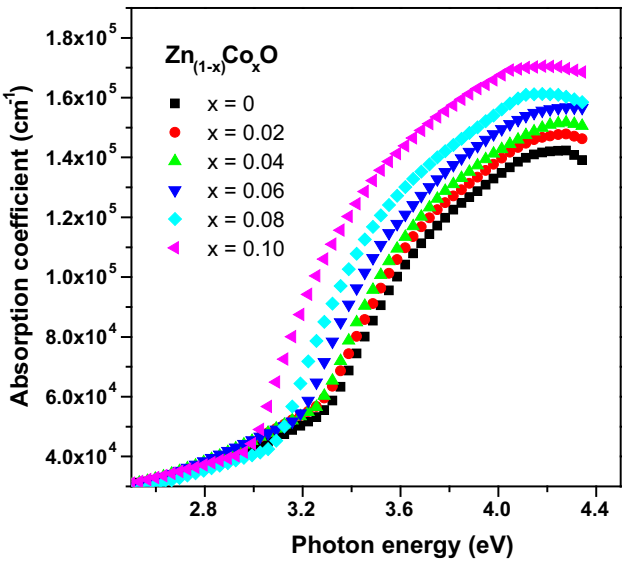

Fig. 12 Variation of the absorption coefficient $\alpha(\lambda)$ versus photon energy ($h\upsilon$) for $Zn_{1-x}Co_xO$ thin films

where the M_i is the molecular weight of the ith component and the X_i is the atomic percentage of the same element in the sample. The density, the molar volume, and the density of polarized constituents are listed in Table 1. The variation of nonlinear refractive index (n_2) with wavelength is given in Fig. 11. It is clear from Fig. 10 that the n_2 increases linearly with increasing n, and the n_2 follows the same trend of n with wavelength, as shown in Fig. 8.

3.2.4 Absorption coefficient and optical energy band gap

The absorption coefficient $\alpha(h\upsilon)$ of $Zn_{1-x}Co_xO$ thin films with different Co concentrations ($x = 0$, 0.02, 0.04, 0.06, 0.08, and 0.1) can be calculated from the values of k and λ using the known formula: $k = \alpha\lambda/4\pi$. Figure 12 shows the variation of $\alpha(h\upsilon)$ as a function of $h\upsilon$. It is known that in the vicinity of the fundamental absorption edge, for allowed direct band-to-band transitions, the $\alpha(h\upsilon)$ is described by:

$$\alpha(h\upsilon) = \frac{K\left(h\upsilon - E_g^{opt}\right)^m}{h\upsilon} \quad (8)$$

where K is a characteristic parameter (independent of photon energy) for respective transitions and m is a number that characterizes the transition process. Many authors [44–47] have suggested different values of m for different glasses: $m = 2$ for most amorphous semiconductors (indirect transition) and $m = 1/2$ for most crystalline semiconductor (direct transition). In few reports, the band gaps of unexposed and exposed samples are classified as a direct transition [48, 49] according to the polycrystalline nature of the XRD samples, as shown in Fig. 3. Therefore, the

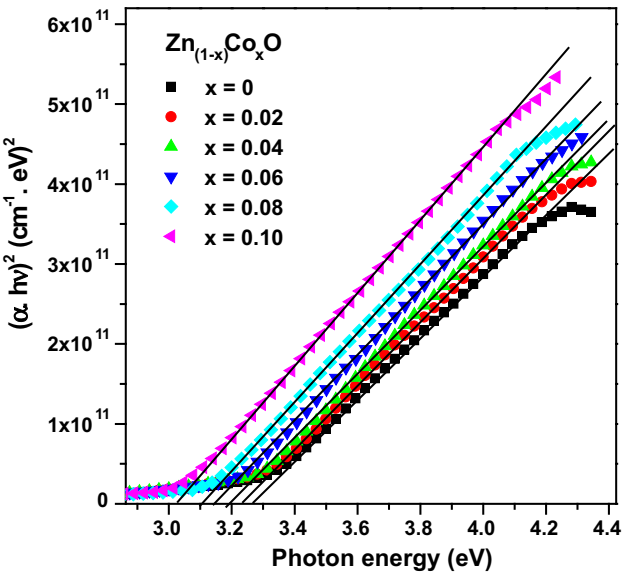

Fig. 13 Plot of $(\alpha h\upsilon)^2$ versus photon energy ($h\upsilon$) for as-deposited $Zn_{1-x}Co_xO$ thin films with different Co concentrations ($x = 0$, 0.02, 0.04, 0.06, 0.08, and 0.1)

allowed direct optical band gaps of unexposed and exposed films are evaluated from $(\alpha h\upsilon)^2$ against $h\upsilon$ plot. Figure 13 shows $(\alpha h\upsilon)^2$ versus $h\upsilon$ plot for different compositions of the $Zn_{1-x}Co_xO$ thin films. The $(\alpha h\upsilon)^2$ versus $h\upsilon$ plot of the thin films exhibits a straight line, and the intercept of the energy axis at $(\alpha h\upsilon)^2 = 0$ gives the direct E_g^{opt}. The variation of direct E_g^{opt} as a function of Co content is listed in Table 1. The values of direct E_g^{opt} are found to decrease with increasing Co content. The decrease in E_g^{opt} for direct transition may be attributed to the decrease in the

crystallite size, because the crystal defects can be formed which produce localized states that change the effective Fermi level due to an increase in carrier concentration [50–52].

4 Conclusions

Bulk samples of the $Zn_{1-x}Co_xO$ ($x = 0$, 0.02, 0.04, 0.06, 0.08, and 0.1) were prepared by a homogeneous precipitation method. TGA was used to identify the calcination temperature for obtaining high-purity $Zn_{1-x}Co_xO$ powder samples. Thin films with the same thickness of different compositions of $Zn_{1-x}Co_xO$ were deposited by thermal evaporation technique in terms of a modified source. The effect of Co content on structural and optical properties of $Zn_{1-x}Co_xO$ thin films was studied. It is observed that the crystallite size varies from 65.36 to 54.72 nm with the increase in Co content in the $Zn_{1-x}Co_xO$ thin films. But the lattice strain increases with increasing Co content. The increasing in lattice strain was attributed to the increase in lattice defects among the grain boundary. The estimated crystallite size using TEM was in a good agreement with that obtained form XRD peaks. The optical properties of the $Zn_{1-x}Co_xO$ thin films were studied from their reflectance and transmittance in the spectral region in terms of Murmann's equation. The refractive index and extinction coefficient have been found to increase with increasing Co content. The increase in the refractive index with Co content has been explained in terms of polarizability. The dispersion of the refractive index was investigated using the WDD single-oscillator model. The oscillator parameters were calculated. The nonlinear refractive index of the $Zn_{(1-x)}Co_xO$ thin films was calculated. The nonlinear refractive index of the $Zn_{(1-x)}Co_xO$ is well correlated with the linear refractive index and WDD parameters which in turn depend on the density and molar volume of the system. The nonlinear refractive index increases linearly with linear refractive index, whereas the nonlinear refractive index follows the same trend of linear refractive index with wavelength.

References

1. D. Mocatta, G. Cohen, J. Schattner, O. Millo, E. Rabani, E. Rabani, U. Banin, Science **1**, 332 (2011)
2. R. Beaulac, L. Schneider, P.I. Archer, G. Bacher, D.R. Gamelin, Science **325**, 973 (2009)
3. A.S. Risbud, N.A. Spaldin, Z.Q. Chen, S.S. Stemmer, Phys. Rev. B **68**, 205202 (2003)
4. M. Bouloudenine, N. Viart, S. Colis, J.D. Kortus, Appl. Phys. Lett. **87**, 052501 (2005)
5. S. Thota, T. Dutta, J. Kumar, J. Phys.: Condens. Matter **18**, 2473 (2006)
6. J.M.D. Coey, M. Venkatesan, C.B. Fitzgerald, Nat. Mater. **4**, 173 (2005)
7. T. Dietl, H. Ohno, F. Matsukura, J. Cibert, D. Ferrand, Science **287**, 1019 (2000)
8. X. Wang, J. Xu, B. Zhang, H. Yu, J. Wang, X. Zhang, J. Yu, Q. Li, Adv. Mater. **18**, 2476 (2006)
9. S.J. Pearton, C.R. Abernathy, M.E. Overberg, G.T. Thaler, D.P. Norton, J. Appl. Phys. **93**, 1 (2003)
10. M. Azarang, A. Shuhaimi, R. Yousefi, M. Sookhakian, J. Appl. Phys. **116**, 084307 (2014)
11. R. Yousefi, F. Jamali-Sheini, M. Cheraghizade, S. Khosravi-Gandomani, A. Sáaedi, N.M. Huang, W.J. Basirun, M. Azarang, Mater. Sci. Semicond. Process. **32**, 152 (2015)
12. I. Khan, S. Khan, R. Nongjai, H. Ahmed, W. Khan, Opt. Mater. **35**, 1189–1193 (2013)
13. K. Rekha, M. Nirmala, M.G. Nair, A. Anukaliani, Phys. B **405**, 3180–3185 (2010)
14. R. Yousefi, A.K. Zak, F. Jamali-Sheini, Mater. Sci. Semicond. Process. (2015) in press. doi:10.1016/j.mssp.2012.12.025
15. X. Peng, B.J. Chu, P.X. Feng, Sens. Actuators B Chem. **174**, 258–262 (2012)
16. C.X. Xu, X.W. Sun, Z.L. Dong, S.T. Tan, Y.P. Cui, B.P. Wang, J. Appl. Phys. **98**, 113513 (2005)
17. J.J. Liu, M.H. Yu, W.L. Zhou, J. Appl. Phys. **99**, 08M119 (2006)
18. Y. Kanai, J. Phys. Soc. Jpn. **24**, 956 (1968)
19. D. Fichou, J. Pouliquen, J. Kossanyi, M. Jakani, G. Campet, J. Claverie, J. Electroanal. Chem. **188**, 167 (1985)
20. X.L. Zhang, R. Qiao, J.C. Kim, Y.S. Kang, Crystal Growth Des. **8**, 2609 (2008)
21. S. Bhattacharyya, A. Gedanken, J. Phys. Chem. C **112**, 4517 (2008)
22. K.F.J. Heinrich, in *Electron beam X-ray microanalysis*, eds. by Von Nostrand Reinhold Co., New York, 1981
23. M. Rathi, P. Ahrenkiel, J. Carapella, M. Wanlass, Microsc. Microanal. **18**, 1046–1047 (2012)
24. B.D. Cullity, *Elements of X-Ray Diffraction*, 2nd edn. (Addition-Weasley, London, 1978)
25. J.I. Langford, A.J.C. Wilson, J. Appl. Cryst. **11**, 102–113 (1978)
26. D.G. Morris, M.A. Morris, M. LeBoeuf, Mater. Sci. Eng., A **156**, 11 (1992)
27. G.H. Chen, C. Suryanarayana, F.H. Froes, Metall. Mater. Trans. **26A**, 1379 (1995)
28. E. Szewczak, J. Paszula, A.V. Leonov, H. Matyja, Mater. Sci. Eng., A **226-228**, 115 (1997)
29. L.A. Agiev, I.N. Shklyarevskii, J. Prekel Spekt. **76**, 380 (1978)
30. N. El-Kabnay, E.R. Shaaban, N. Afify, A.M. Abou-sehly, Phys. B **403**, 31 (2008)
31. O.S. Heavens, *Optical Properties of Thin Films* (Dover, New York, 1965)
32. S. Tolansky, *Multiple-Beam Interference Microscopy of Metals*, vol. 55 (Academic Press, London, 1970)
33. S.R. Elliott, *The physics and chemistry of solids* (Wiley, Chichester, 2000)
34. S.H. Wemple, M. DiDomenico, Phys. Rev. B **3**, 1338 (1971)
35. T. Tanaka, Thin Solid Films **66**, 271 (1980)
36. S.H. Wemple, M. DiDomenico, Phys. Rev. B **3**, 1338 (1971)
37. M. El-Hagary, M. Emam-Ismail, E.R. Shaaban, S. Althoyaib, Mater. Chem. Phys. **132**, 581 (2012)
38. P. Sharma, S.C. Katyal, J. Appl. Phys. **107**, 113527 (2010)
39. H. Ticha, L. Tichy, J. Optoelectron. Adv. Mater. **4**, 381 (2004)
40. J. Fournier, E. Snitzer, The nonlinear refractive index of glass. IEEE J Quantum Elect. **10**, 473–475 (1974)
41. C. Wang, Phys. Rev. B **2**, 2045 (1970)

42. M. Asobe, T. Kanamori, K. Kubodera, IEEE J. Quantum Electron. **29**, 2325 (1993)
43. T. Topfer, J. Hein, J. Phillipps, D. Ehrt, R. Sauerbrey, Appl. Phys. B Lasers Opt. **71**, 203 (2000)
44. E.A. Davis, N.F. Mott, Philos. Mag. **22**, 903 (1970)
45. E. Márquez, J.M. González-Leal, A.M. Bernal-Oliva, R. Jiménez-Garay, T. Wagner, J. Non-Cryst. Solids **354**, 503 (2008)
46. E.R. Shaaban, Philos. Mag **88**, 781 (2008)
47. E.R. Shaaban, M. Abdel-Rahman, El Sayed Yousef, M.T. Dessouky, Thin Solid Films **515**, 3810 (2007)
48. P. Pramanik, S. Bhattachraya, J. Electrochem. Soc. **137**, 3869 (1990)
49. R.H. Misho, W.A. Murad, G.H. Fatahalah, I.M. Abdul-Aziz, H.M. Al-doon, Phys. Stat. Solidi (a) **109**, K101 (1988)
50. E.R. Shaaban, Appl. Phys. A **115**, 919 (2014)
51. E.R. Shaaban, I. Kansal, S.H. Mohamed, J.M.F. Ferreira, Phys. B Condens. matter **404**, 3571 (2009)
52. E.R. Shaaban, J. Alloys Compd **563**, 274 (2013)